Unveiling the Underlying Influence of pH on the Crystallization of Hybrid Perovskite Materials, Delivering Low Voltage Loss Photovoltaics

Nakita K. Noel,[1] Martina Congiu,[1,2] Alexandra J. Ramadan,[1] Sarah Fearn,[3] David P. McMeekin,[1] Jay B. Patel,[1] Michael B. Johnston,[1] Bernard Wenger[1*], Henry J. Snaith.[1*]

[1] Clarendon Laboratory, Department of Physics, University of Oxford, Parks Road, Oxford, OX1 3PU, United Kingdom

[2] Centre for Nanoscience and Technology, Italian Institute of Technology, via Giovanni Pascoli 70/3, Milano 20133, Italy

[3] Department of Materials, Imperial College London, London, SW7 2AZ, United Kingdom

[*] Corresponding authors: henry.snaith@physics.ox.ac.uk, bernard.wenger@physics.ox.ac.uk

Abstract:

Impressive power conversion efficiencies coupled with the relative ease of fabrication, have made perovskite solar cells a front-runner for next generation photovoltaics. While perovskite films and optoelectronic devices have been widely studied, relatively little is known about the chemistry of the precursor solutions. Herein, we present a study on the hydrolysis of N, N-Dimethylformamide (DMF), correlating how the pH changes related its degradation affect the crystallisation of $CH_3NH_3PbI_{3-x}Cl_x$ perovskite films. By careful manipulation of the pH, and resultantly the colloid distribution in the solution, we process perovskite films with greatly improved crystallinity. Upon incorporation of these films into photovoltaic devices, we reproducibly achieve power conversion efficiencies of over 18%. Furthermore, through the application of this method to the mixed-cation, mixed-halide perovskite

$FA_{0.83}MA_{0.17}Pb(I_{0.83}Br_{0.17})_3$, we are able to achieve power conversion efficiencies of up to 19.9% and open-circuit voltages of 1.21 V for a material with a bandgap of 1.57 eV, which yields the lowest yet reported loss-in-potential from bandgap to V_{OC} of only 360 mV.

Introduction:

During the last five years, organic-inorganic lead halide perovskites have become a major focal point of the research community. These materials have shown applications in both light emitting diodes[1, 2] and lasers;[2] but most notably, have leapt to the forefront of emerging photovoltaic technologies, achieving certified power conversion efficiencies (PCE) of up to 22.1%.[3] Lead halide perovskite materials have shown themselves to be efficient absorbers,[4] but are also capable of generating free carriers and transporting charge.[5-7] This has allowed the exploitation of this material in various solar cell architectures, from mesoscopic to planar heterojunction devices.[8]

One of the main selling points of this material is the wide range of methods through which high-quality, crystalline films can be produced. These include a variety of solution deposition processes,[4, 5, 9, 10] vapour deposition,[11, 12] and mixtures of the two.[10] To date, solution deposition methods, specifically spin-coating from either DMF (one step spincoating) or mixtures of DMF and DMSO (anti-solvent quenching), remain the most widely used deposition methods for the production of lab-scale perovskite devices. Through the careful fine-tuning of the specific perovskite composition and deposition methods, as well as the manipulation of the solvent through the use of compound solvents and solvent mixtures,[13-16] the PCEs of perovskite-based photovoltaics have soared. However, most efforts to increase

the PCE have relied upon empirical processing parameter optimisation, and relatively little attention has been paid to understanding the chemistry of the precursor solution, and how and why this affects the crystallization of perovskite films.

There have been numerous reports of the introduction of additives to precursor solutions as a means of influencing the crystallisation and optoelectronic properties of perovskite films. Such additives include various metal cations,[17, 18] halide and phosphorous acids,[19-22] ionic liquids,[23] organic small molecules, [24] and even water.[25] In all cases, the inclusion of small concentrations of these materials in the precursor solution has not only been shown to increase the surface coverage and improve the crystallinity of the perovskite films, but also to enhance the optoelectronic properties of the material. In particular, acids are widely used as additives to the perovskite precursor solution. We have previously shown an increase in film quality upon addition of hypophosporous acid (HPA) to a lead acetate-based methylammonium lead iodide ($CH_3NH_3PbI_3$) precursor solution,[20] the use of hydroiodic acid (HI) to improve the film morphology of formamidinium lead iodide ($CH(NH)_2PbI_3$),[26] and reduce the crystallisation temperature of $CsPbI_3$[19] and more recently, using a mixture of HI and hydrobromic acid (HBr) introduced a method of controlling the crystallisation kinetics of formamidinium-cesium mixed-cation mixed-halide perovskite, via manipulation of the colloidal concentration in the precursor solution.[27] There have however, been differing reports as to the optimal concentration of acid to add to perovskite precursor solutions,[19, 21, 26, 28] as well as concerns as to how the addition of excess halide affects the overall perovskite stoichiometry and thus, its optoelectronic properties. [29]

One of the most important factors in the solution-based crystallisation of any material is the solubility of the precursor salts in the chosen solvent. In the case of the salts required for

perovskites, this solvent is typically N, N-dimethylformamide (DMF), or a combination of DMF and dimethyl sulfoxide (DMSO). In its anhydrous state, DMF is a relatively neutral solvent with a pH of 6.3 which, upon exposure to water, undergoes hydrolysis to produce formic acid (FAH) and dimethylamine (DMA).[30-32] When DMF has been hydrolysed and is in equilibrium with its degradation products, the solvent becomes basic, having a pH of approximately 11.[33] We have previously observed, in the growth of single crystals of the $CH_3NH_3PbI_3$ perovskites, that the time and temperature required for the mother liquor to reach supersaturation and produce crystals, is dependent on the age, and consequently, pH of the solvent.[34] In this case, when using anhydrous DMF, the addition of formic acid was seen to decrease both the time and the temperature at which crystallisation of the perovskite occurred. Through the addition of formic acid to anhydrous DMF, we can control the pH of the solvent, and as such, the solubility of the precursor salts. We postulate that by applying this methodology to the precursor solution for thin-film fabrication, we can have more precise control over the crystallisation of perovskite films, and as such, greater reproducibility in device performance.

Herein, we carry out a spectrophotometric investigation of the changes in pH of both neat and acidified DMF as it undergoes hydrolysis. We show how these changes in pH affect the ability of the solvent to solvate the perovskite precursor salts, and what effect this has on the resultant perovskite films. By utilising formic acid to artificially tune the 'age' of the DMF, we can control the crystallisation of $CH_3NH_3PbI_{3-x}Cl_x$ films, to obtain reflective, pinhole free films. Upon incorporation of these films into devices, we show enhanced power conversion efficiencies of over 18%, and a significant decrease in the standard deviation of the PCE. To investigate whether there is an added advantage to utilising this approach in a slightly more controlled, fast crystallization process, or with a different perovskite composition, we apply

this method to the widely used solvent quenching process. Here, through the addition of formic acid to a precursor solution of the mixed cation, mixed halide perovskite $FA_{0.83}MA_{0.17}Pb(I_{0.83}Br_{0.17})_3$, we see a marked increase in the photoluminescence quantum efficiencies (PLQE) of the films produced. Incorporating these films into photovoltaic devices yields stabilised efficiencies of up to 19.9% and open circuit voltages of up to 1.21 V, showing a remarkably low voltage loss of just 360 mV. By manipulating the solvent pH, we achieve a further 30 mV decrease on the best reported loss-in-potential from bandgap to V_{OC} of 390 mV. [35]

Results and Discussion:

The pH of a solution can be determined via two main pathways, through spectrophotometric or potentiometric analysis. The potentiometric determination of the pH of a solution is often used in cases where the solution under investigation is ion rich. Here, however, where our solution is in an organic solvent which is ion deficient, the results obtained through this method of analysis may be confounded by diffusion of the ions from the reference electrode into the test solution, potentially introducing significant ambiguity. With this in mind, we have used spectrophotometric analysis to investigate any changes in the pH of DMF due to either hydrolysis, or the addition of acids to the solvent.

For these experiments we use thymol blue as a pH indicator in DMF. Under strong acidic conditions, this indicator has a strong red/pink colour (absorption peak at 550 nm) which transitions to yellow (absorption peak at 402 nm), and then blue (absorption peak at 615 nm)

in neutral to slightly alkaline and highly alkaline environments respectively.[36] We show the chemical structures of thymol blue in different pH regimes in **Figure 1**, along with the absorption spectra obtained in acidified, neutral and alkalinized solutions of DMF.

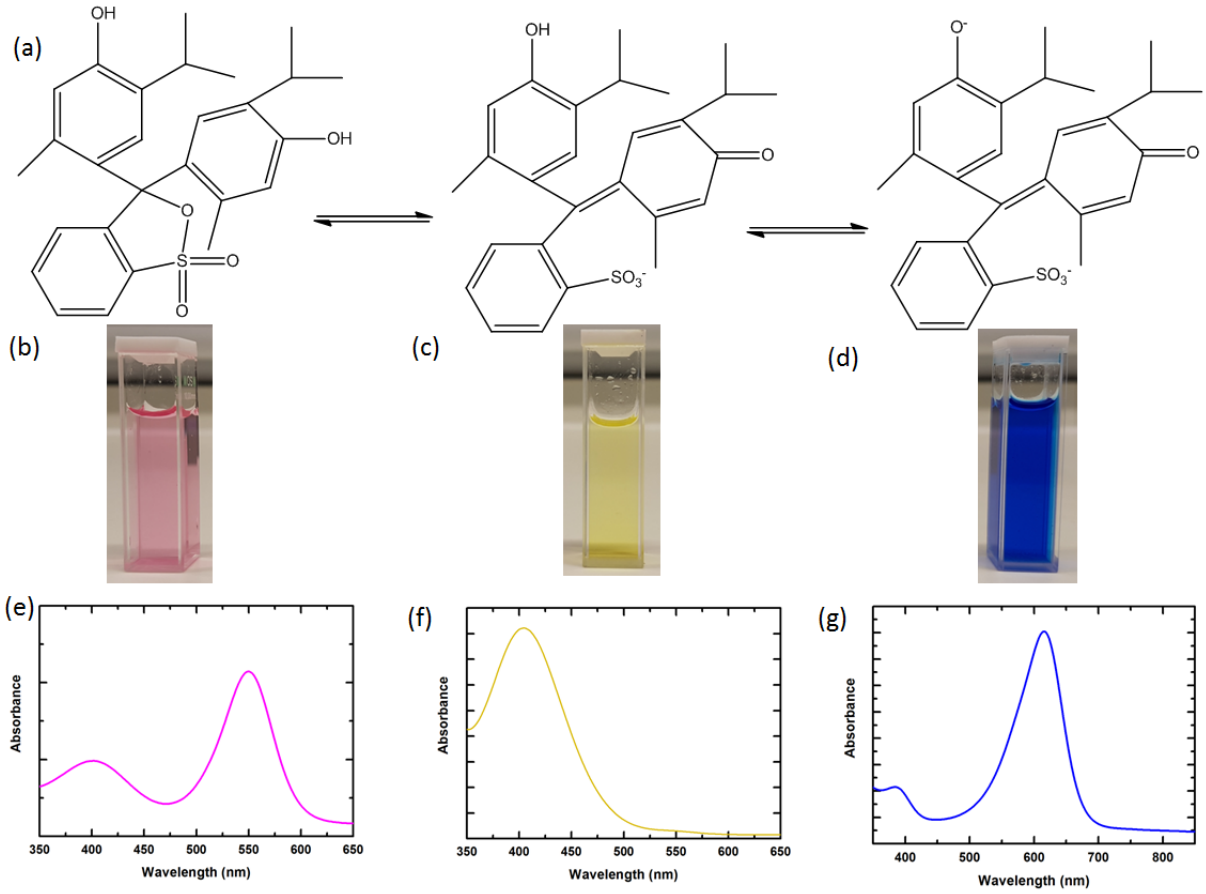

Figure 1: **Chemical Structure and Absorption Spectra of Thymol Blue**. (a) Chemical structures of thymol blue in (from left to right) acidic, neutral and basic environments. (b), (c) and (d) Photographs of thymol blue in (from left to right) acidified DMF, neat DMF, and alkalinized DMF. (e), (f) and (g) Absorption spectra of the solutions shown in (b), (c) and (d) respectively.

In Fig.1f we show the absorption of thymol blue in a neutral environment, where we observe that the most prominent absorption peak is at 402 nm. This peak is most visible under neutral or weakly basic conditions. In order to speed up the rate of hydrolysis of DMF, we subject the solvent to temperature cycling, gradually increasing the temperature from 25 °C to 95 °C,

followed by gradually cooling the solution back down to 25 °C, over a period of 45 min. As aforementioned, when DMF is hydrolysed the pH of the solution moves towards a more basic regime. As such, we expect that as this occurs, we should see a decrease in the absorption peak at 550 nm, and a subsequent increase in the peak at 402 nm (see Fig.1a). Thus, to investigate the pH change that occurs as a consequence of this hydrolysis, we measure the change in the absorbance at 402 nm as a function of time and temperature. We present the results in **Figure 2**. In the first step of the temperature cycle, the absorbance remains constant as the solution is held at 25 °C for 2 min. The second step of the cycle involves a gradual increase in temperature over approximately 15 min to 95 °C, during which we see a decrease in the absorbance at 402 nm. This decrease in the absorbance indicates that the solution becomes less basic. The chemical reaction for the hydrolysis of DMF is described by **Equation 1**:

$$HCON(CH_3)_2 \underset{}{\overset{H_2O}{\rightleftharpoons}} HCOOH + (CH_3)_2NH \qquad (1)$$

With increasing temperature, the equilibrium position of the above reaction shifts to the right, thus producing more formic acid and dimethylamine. As discussed by Nayak, Moore and co-workers, when considering the influence of temperature upon the crystallisation of large single crystals from solution, we expect that the temperature increase will also encourage the dissociation of the formic acid, thus decreasing the basicity of the DMF solution.[34] In the third step of the temperature cycle, the DMF is held at 95 °C for 5 min. At this point, we see the solution very slowly begins to recover, experiencing a small increase in basicity. The final step of the temperature cycle involves a gradual return to room temperature, during which we see the solution become increasingly basic, even more so than before the temperature cycling.

We can interpret these results to indicate that while increasing the temperature results in an increase in acidity (or decrease in basicity) due to the reversible dissociation of formic acid; subsequent to the heating cycle, the DMF becomes more basic than in its anhydrous state, most likely due to hydrolysis having occurred. This is consistent with the formation of dimethylamine which has a lower pK_a ($pK_a^{conj.\ acid}$ = 10.4 in DMF) than of formic acid (pK_a = 18.9 in DMF).[37] This means that dimethylamine is a stronger base than formic acid is an acid, and thus, when they are both present in similar concentration, dimethylamine would have a larger influence on the pH of a solution. In Fig. 2b, we show the progressive changes in the 402 nm absorbance of thymol blue in DMF for four consecutive heating cycles. The solution was left to rest at 25 °C for one hour between each heating cycle. Here, we see that the increase in basicity which occurs after temperature cycling is irreversible. Even when the solution is left to rest, it does not appear to recover, with the pH of the solution at the beginning of the second cycle being exactly the same as it was at the end of the first cycle.

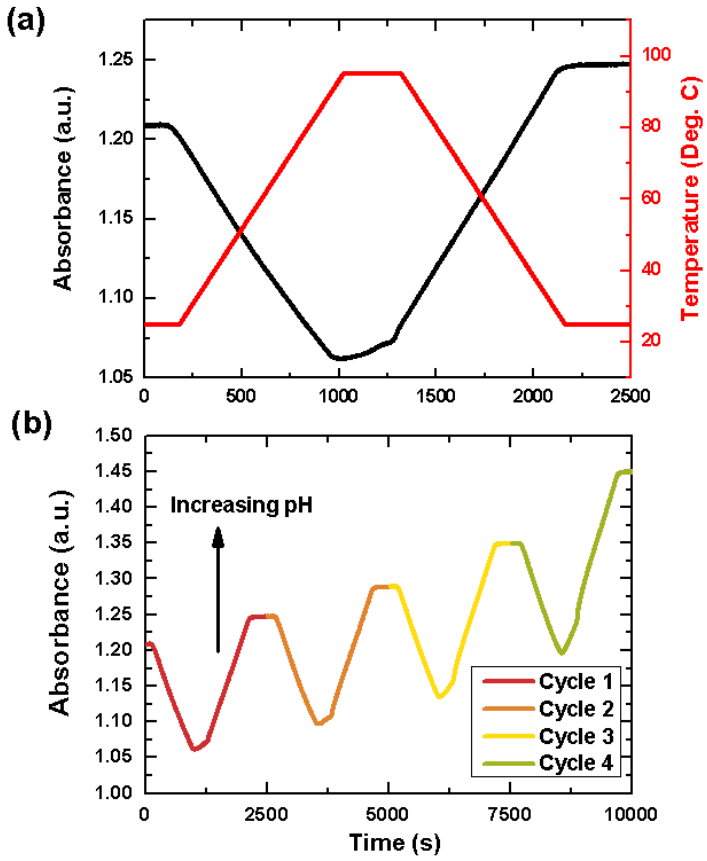

Figure 2: Temperature Cycling of DMF. (a) Evolution in the absorbance of thymol blue in DMF at 402 nm, with time and temperature. The change in absorbance is depicted by the solid black line and the corresponding temperature curve is shown by the dashed red line. (b) The change in 402 nm absorbance of thymol blue in DMF over four successive temperature cycling events. Note that the higher absorbance on each cycle corresponds to the lower temperature of 25 °C.

This trend continues for all subsequent temperature cycles, with the change in absorbance, and thus pH, becoming greater as the cycling continues. Another interesting feature of these temperature dependent measurements is how the solution behaves when held at high temperature. We see the increase in absorbance which occurs when the solution is held at 95 °C becoming steeper with each cycle. During the course of this measurement, we expect that the decrease in absorbance is due to the deprotonation of formic acid with an increase in

temperature. However, the gradual increase in absorbance which we see when the solution is held at high temperature is likely due to the fact that with each temperature cycle, the hydrolysis of DMF is being pushed closer and closer to its equilibrium point. This will create an increasingly more basic solution, which when held at a constant high temperature, proceeds more quickly to its equilibrium point. Indeed, if we hold the solution at high temperature over a period of hours, we see the absorbance continue to increase until it reaches a plateau, which we attribute to the hydrolysis reaching equilibrium conditions (See **Figure S1**).

We now consider the effect of acidic additives on the pH of DMF. There have been various reports of the use of acids as an additive to the perovskite precursor solution, all showing improved crystallisation, as measured by increased the surface coverage of the perovskite films on the substrates, and enhanced device performance in solar cells. Here, we use HCl, HPA and formic acid to determine what, if any, effect they have on the pH of DMF. While HI is the most commonly used acid additive for $CH_3NH_3PbI_3$ solutions, it has recently been shown that it can result in slight shifts in the bandgap of the material.[29] For this measurement, we have not investigated HI as an additive due to the fact that the triiodide absorption peak overlaps with the absorption of thymol blue, making it difficult to disentangle pH effects from the oxidation of iodide ions. We show our results for the addition of formic acid to DMF in **Figure 3**.

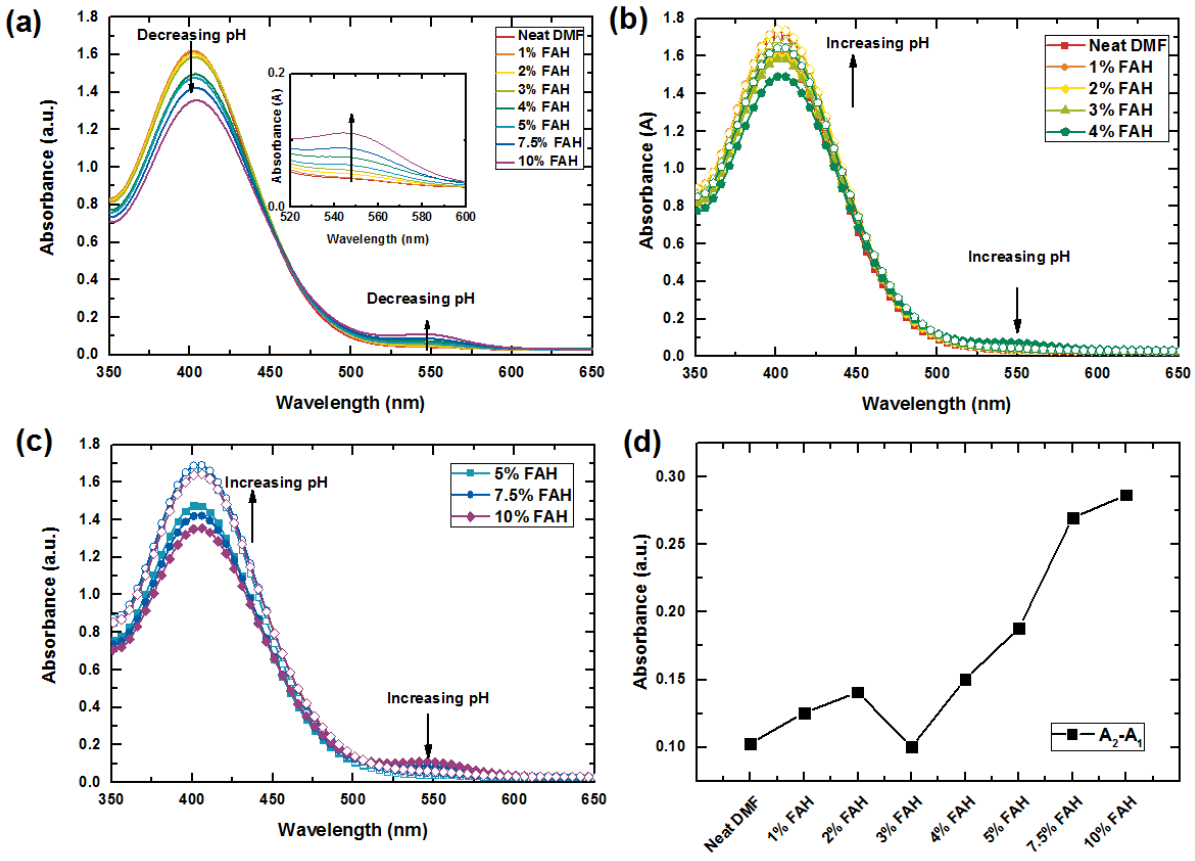

Figure 3: Addition of Formic Acid to DMF. (a) Absorption spectra of thymol blue in DMF with the addition of increasing amounts of formic acid (FAH). A close up of the changes in the 550 nm absorption peak is shown in the inset. (b) and (c) Absorption spectra of thymol blue in acidified DMF before and after temperature cycling. Solid symbols show the absorption before cycling and open symbols depict the spectra after temperature cycling. (d) Change in the value of the 402 nm absorption peak before and after temperature cycling.

In Fig. 3a we see that when in neat DMF, the absorbance of thymol blue at 550 nm is negligible, but with the addition of increasing volumes of formic acid, we observe a decrease in the absorbance at 402 nm and a corresponding increase in the absorbance at 550 nm. This is expected to occur as the solution becomes increasingly acidic. Interestingly however, we see that after temperature cycling these solutions (see Figs. 3b and 3c), the higher the acid concentration used, the more basic the solution becomes. This is more clearly seen in Fig. 3d

where we show the difference in the 402 nm absorbance before (A_1) and after (A_2) temperature cycling. We observe a similar trend for the addition of the more common acidic additives such as HCl and HPA (See **Figure S2**). Strong acids such as the hydrohalic acids are very commonly used as catalysts in the hydrolysis of DMF.[38] The stark increase in the basicity of the solution with the addition of large amounts of acid can therefore be explained by an increase in the rate of hydrolysis of the DMF, and the resultant increase in the concentration of dimethylamine present in the cycled DMF. The hydrolysis of DMF is typically a slow process, and an interesting point to note is that the simple addition of deionized water is not enough to produce such a rapid change in the pH of the DMF. This excludes the possibility that, on this timescale, these effects are simply due to the water content of the given acids (see **Figure S3**). Another point of note is that while the addition of formic acid, deionized water and HCl to DMF results in very similar absorption profiles when subjected to temperature cycling, the addition of HPA appears to result in an almost immediate and continuous increase in basicity with temperature (See **Figure S4**).

We, and others, have previously shown that precursor solutions of perovskite materials contain colloidal dispersions, rather than being entirely composed of fully solvated ions.[27, 34, 39] Having shown here that the addition of acid changes the composition of DMF as a solvent, and irreversibly changes the pH, we now investigate how this affects its ability to solvate the perovskite precursor salts. In order to do this, we prepare precursor solutions of $CH_3NH_3PbI_{3-x}Cl_x$ in DMF at 38 wt.% (3M MAI: 1M $PbCl_2$) and do dynamic light scattering (DLS) measurements on the neat solution, as well as on solutions with acidic additives. We present the results of these measurements in **Figure 4**. We note here that while the absolute pH of the full solution (DMF+salts) will not be exactly the same as for the neat and acidified DMF

without salts, the important metric is the overall change or variation in the pH of the solution which results from using DMF in different stages of hydrolysis.

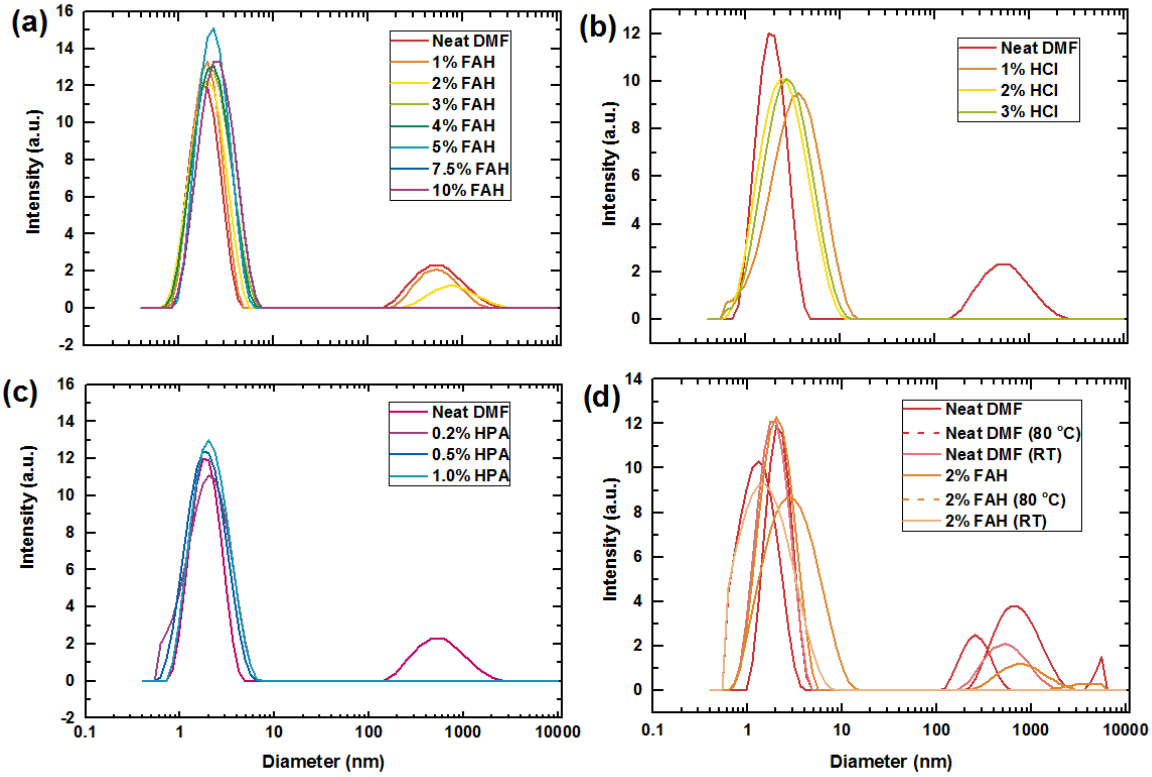

Figure 4: Dynamic Light Scattering Measurements. Change in the size distribution of colloids present in a 38 wt.% precursor solution of $CH_3NH_3PbI_{3-x}Cl_x$ with the addition of (a) formic acid (FAH), (b) HCl, and (c) HPA. (d) Change in the size distribution of colloids with heat, and both heat and acid. Solid traces show the measurements taken before heating, and after being heated and cooled down to room temperature (RT), while dashed lines show the colloidal distribution at 80 °C.

From the results shown in Fig.4, we see that in the neat precursor solution, without the addition of acid, there are some large (hundreds of nm) colloids, along with smaller colloids with diameters between 1 and 10 nm. It is important to note that the overall concentration of the perovskite precursor solution was kept constant for all experiments. For example, the neat solution was made such that 38 wt.% of the precursor salts was dissolved in 1 ml of DMF.

Similarly, for the 1% FAH solution, the same mass of salts was dissolved in 1 ml of solvent (990 μL DMF+ 10 μL FAH). With the introduction of 1 vol.% FAH and 2 vol.% FAH, we observe a successive decrease in the number of larger colloids present in the solution. Upon the addition of 3 vol.% FAH, these larger colloids completely disappear, suggesting that at this point, we have very close to a true solution, or at least a solution of solvated small complexes and ions. With a stronger acid such as HCl, the addition of 1 vol.% of acid to the precursor solution is enough to entirely remove the presence of larger colloids. In the case of HPA, we see that the addition of just 0.2 vol.% of HPA to the precursor solution completely rids the solution of the presence of large colloids. This coincides with the previous observations that the addition of 3-5 μL of HPA to 1 ml of a perovskite precursor solution have been sufficient to result in a significant enhancement in film quality.[20]

We have previously shown the dissolution of colloids in perovskite precursor solutions with increasing temperature.[34] Here, we investigate the effects of temperature on the presence of colloids in a neat precursor solution, as well as in a solution to which we have added formic acid. We initially measure the solution at 25 °C, then heat the solution to 80 °C and re-measure it. Subsequently, we allow the solution to cool down to room temperature, and then take a final set of measurements. We note that while there are both small and larger colloids present in the neat DMF solution, upon heating the solution up to 80 °C, we observe that both the size and number of these colloids decrease. However, when the solution is cooled to room temperature, it returns to a point close to its original state, albeit with a smaller proportion of larger colloids. For the acidified solution, we chose to add 2 vol. % FAH, as at this acid concentration there are still a few large colloids present in the solution. Here, when we heat the solution we observe a similar trend as with the neat DMF solution; a significant decrease in number of large colloids present in the solution. Interestingly, when we allow this acidified

solution to cool down to room temperature, it does not return to its original state. Rather, we no longer detect the large, micron sized colloids, and observe that in addition the distribution of smaller colloids or complexes have shifted towards smaller diameters. This indicates that heating the solution in the presence of formic acid causes it to go through an irreversible change, which effectively allows the solvent to better solvate the precursor salts.

We know from our previous work, that heating a solution of perovskite precursor salts in DMSO causes the deprotonation of the methylammonium cation to form methylamine, which has been shown to be an excellent solvent for perovskite salts.[13, 34, 40] This process is likely the cause of the decrease in the number and distribution of colloids which we see in both the neat and acidic precursor solutions. However, since this process should be completely reversible upon cooling, these results suggest that there is another mechanism at play, and points to the role of DMF as a solvent. We have seen from the temperature cycling measurements which we have shown in Figs. 1 and 2, that as DMF is hydrolysed it becomes increasingly basic due to the formation of dimethylamine. The rate of hydrolysis of DMF also appears to increase with the addition of acid.[31] We propose that the dimethylamine produced by the hydrolysis of DMF, as with other amines which we have previously investigated,[13] increases the solvating power of DMF, making it a better solvent for the perovskite precursors. To test this theory, we bubble dimethylamine into the precursor solution using a method which we have previously described for bubbling methylamine into solvents.[13] We see that for time intervals as short as 1 min, there is a large reduction in the size and number of colloids which are present in the precursor solution, consistent with our hypothesis that the generation of dimethylamine in decomposed DMF is the most likely cause of further colloid dissolution (See **Figure S5**).

Controlling the distribution of colloids in a perovskite precursor solution has been shown to be extremely important to the morphology of the final film.[27, 39] In the present work, we have seen that the addition of formic acid to the perovskite precursor solution results in the dissolution of colloids. By starting with a concentration of formic acid for which all large colloids are dissolved (3% FAH), we are able to reproducibly obtain specular, pinhole free films with larger, more highly oriented crystals. We present images of such films and X-ray diffraction data in **Figure 5**.

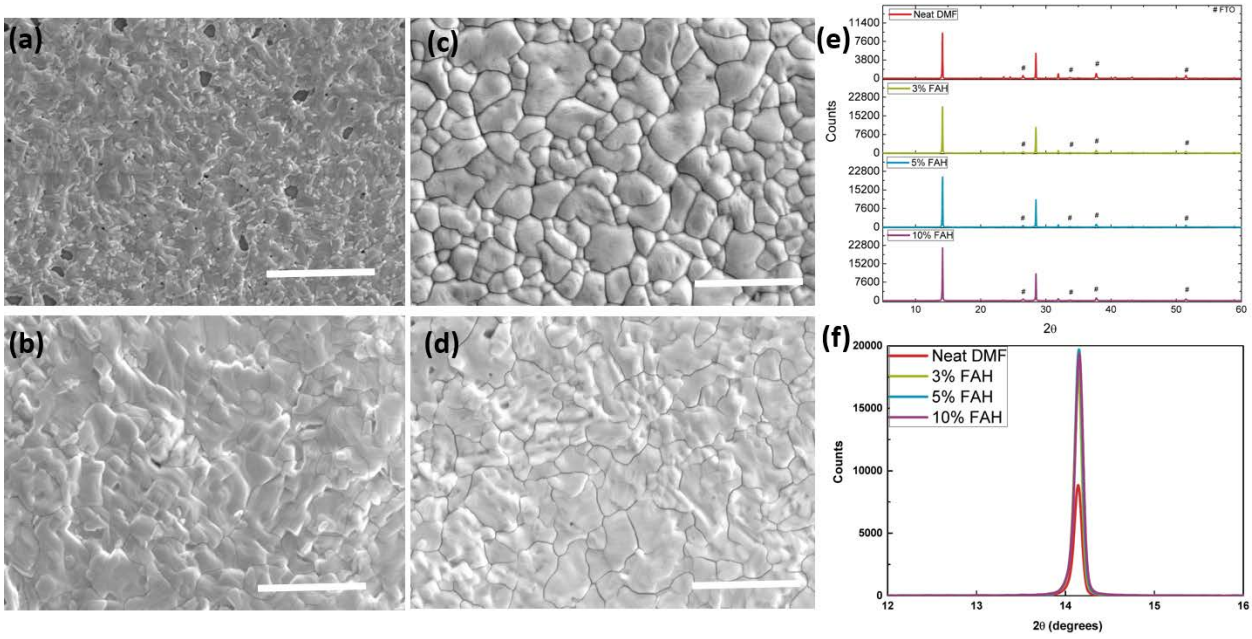

Figure 5: Scanning Electron Microscopy and X-Ray Diffraction. (a)-(d) Top-view SEM images of $CH_3NH_3PbI_{3-x}Cl_x$ perovskite films coated from neat and acidified DMF solutions, with formic acid additions of 0 µL, 30 µL, 50 µL, and 100 µL/mL respectively. The scale bars on all images represent a distance of 5µm. (e) X-ray diffractograms of films from control and acid modified solutions. (f) Close-up view of the 110 peak of the perovskite films shown in (e).

In Fig.5, we show top view SEM images and the corresponding diffractograms of $CH_3NH_3PbI_{3-x}Cl_x$ films formed on fluorine-doped tin oxide (FTO) substrates coated with a compact layer of crystalline SnO_2, [41] from precursor solutions made with neat and acidified

DMF. While we observe a few pinholes present in the film that we processed from the neat solution, we observe no visible pinholes in films which we have processed from solutions containing formic acid. Furthermore, we begin to see more defined crystal domains. To assess the crystallinity of the films we have performed XRD measurements on these films, and find that the addition of formic acid results in a significant increase in the crystallographic texture of the film, as is evidenced by the doubling of the intensity of the 110 peak. It is interesting to note that while there is almost a doubling of the intensity of the 110 peak when 3 vol.% of formic acid is added to the solution, this increase does not continue linearly as more acid is added. We observe similar effects (i.e. increased surface coverage and increased crystallinity and/or orientation of the grains) for the addition of halide acids, but at different concentrations (See **Figure S6**). We note however, that while we observe an increase in surface coverage for some concentrations of the halide acids, we do not completely eliminate pinholes in the films we have fabricated using halide acids. We show these results for different acids in **Figure S7**. It has recently been reported that aging the $CH_3NH_3PbI_3$ perovskite precursor solution at 70 °C for 48 hrs is beneficial for film formation, in that it allows the production of pinhole free films with large crystalline domains.[42] We believe that this observation is largely due to the dissolution of colloids in the precursor solution, which occurs as a result of changes to the solvent. Both the application of heat and the addition of acids to DMF cause an artificial 'aging' of the solvent, causing in the onset of degradation of DMF which results in the production of dimethylamine. Dimethylamine is produced through both the thermal degradation and the hydrolysis of DMF, allowing for, in both cases, the dissolution of colloids in the precursor solution. We propose that the "universal" improvements which have been seen in $CH_3NH_3PbI_3$ perovskite solar cells, as a result of the addition of acids[19-21] and water to the precursor solution, and even through the popular deposition method of hot-casting,[42-44] are due mainly to the dissolution of

colloids, with the latter occurring as a result of changing the chemistry of the solvent and increasing its solvation power.

To ascertain the effects that using different acidic additives in the perovskite precursor solution have on the composition of the resultant film, we have carried out depth profiling time-of-flight (ToF) secondary ion mass spectrometry (SIMS) on films fabricated using equal volumes of the most common acid additives, as compared to formic acid. The results of these measurements are presented in **Figures S8-S10**, and show that while films formed using neat DMF and DMF + formic acid solutions are incredibly similar, films formed in the presence of other acid additives indicate the inclusion of phosophorus or excess halide in the films.

Having shown the effect of manipulating the pH of DMF on colloid concentration, and thus film quality, we proceed to investigate how this affects the operation when the perovskite films are incorporated into solar cells. In order to do this, we fabricate planar heterojunction solar cells using the device structure FTO/SnO_2/$CH_3NH_3PbI_{3-x}Cl_x$/spiro-OMeTAD/Ag. We present these results in **Figure 6**. In Figure 6a we show statistics collected from 8 different batches of experiments (the complete performance parameters are shown in **Figure S11**). Here we see that the addition of formic acid results in a steady increase in the PCE, peaking with the addition of 5 vol.% formic acid, after which there is a decrease in the mean efficiency. Notably we observe the average PCE to increase from 14% to 18% with the addition of formic acid. We see a similar trend with the direct addition of dimethylamine (**Figure S12**). We give the performance parameters of the devices in **Table 1**. In Fig.6b we show the current-voltage curves of the champion control device, fabricated with the neat solution, at an efficiency of 17.7%, as well as the champion device for the optimised

concentration of formic acid, for which we measure a power conversion efficiency of 18.8%. We note that while both of these devices show hysteresis in the current-voltage curves, the degree of hysteresis is reduced with the addition of the formic acid (See **Figure S13**). We present the steady-state maximum power point current density and PCE of these devices in Figs.6c and 6d, which also shows an increase from 17.0 to 18.3% with the addition of formic acid. The external quantum efficiency (EQE) of the champion devices is shown in **Figure S14**. Notably, in addition to a significant increase in the overall power conversion efficiency, we also observe a much narrower distribution of performance for the cells with the optimum addition of formic acid, with an increase in the average efficiency and reduction in the standard deviation from 13.8 ± 1.5% to 18.3 ± 0.5%. We also note that, as far as we are aware, this is the highest steady state efficiency reported to-date for a planar heterojunction perovskite solar cell employing a perovskite layer which is spin-coated from a DMF-based solution via a simple one-step spin-coating process, without additional air-drying or solvent quenching during coating.

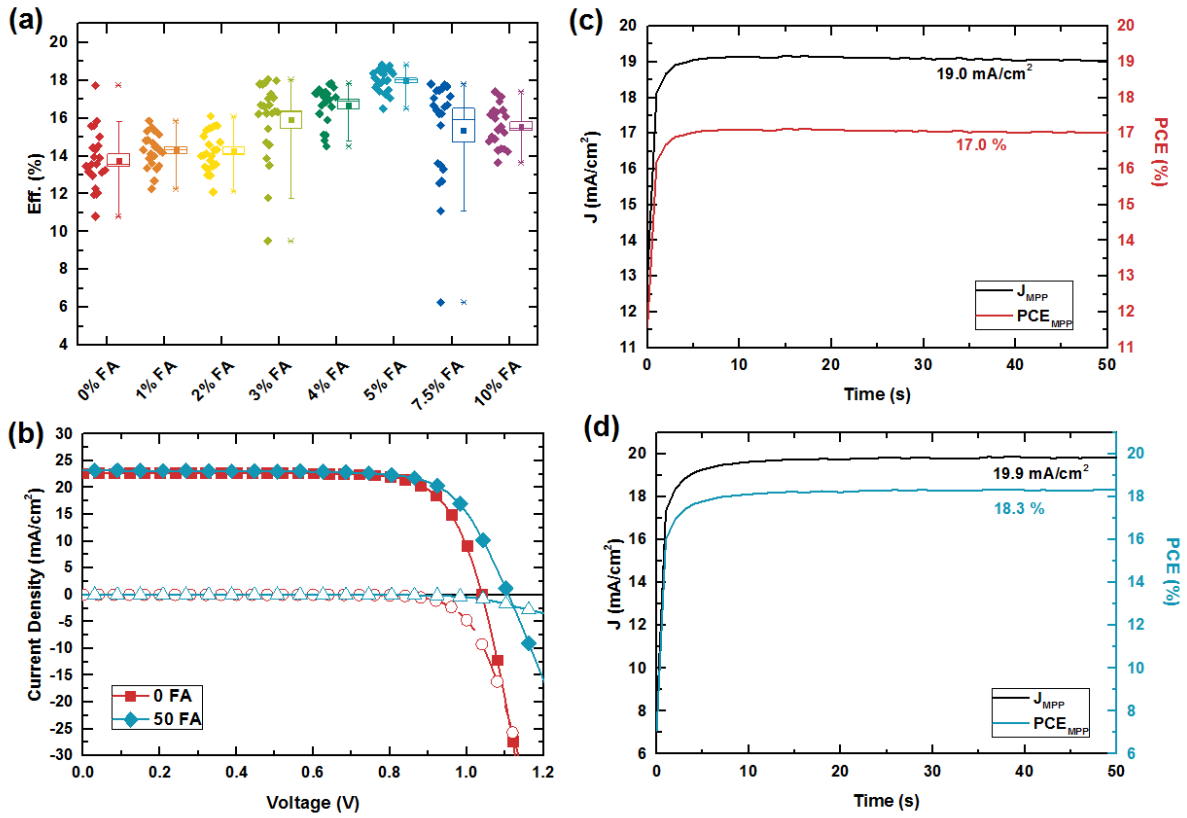

Figure 6: Current-Voltage Characteristics. (a) Statistics on the efficiency of 8 individual batches of solar cells prepared using neat and acidified DMF, using from 0 to 10 vol. % of formic acid as an additive to the precursor solution. (b) Current-Voltage curves of solar cells fabricated using neat DMF as a solvent, as well as DMF with 5 vol.% of formic acid added. (c) and (d) Stabilised current density and PCE of the devices shown in (b). These measurements are taken by holding the devices at their maximum power point over a period of 50 seconds.

[FAH]	J_{SC} (mA/cm^2)	η (%)	V_{OC} (V)	FF (a.u.)	η_{MPP} (%)
0	20.8 ± 1.4 (22.6)	13.8 ± 1.5 (17.7)	1.02 ± 0.04 (1.04)	0.64 ± 0.04 (0.74)	17.0
10	19.5 ± 1.1 (20.9)	14.3 ± 0.9 (15.9)	1.05 ± 0.08 (1.04)	0.69 ± 0.03 (0.72)	
20	20.0 ± 1.0 (21.5)	14.2 ± 1.0 (16.1)	1.06 ± 0.04 (1.07)	0.67 ± 0.03 (0.69)	

30	22.1 ± 1.0 (23.2)	15.9 ± 2.1 (18.0)	1.05 ± 0.03 (1.04)	0.68 ± 0.07 (0.75)	
40	22.7 ± 1.2 (23.8)	16.7 ± 1.0 (17.9)	1.06 ± 0.03 (1.05)	0.70 ± 0.01 (0.71)	
50	23.0 ± 0.5 (23.2)	18.3 ± 0.5 (18.8)	1.11 ± 0.02 (1.10)	0.72 ± 0.02 (0.74)	18.3
75	22.2 ± 1.5 (23.3)	15.3 ± 2.5 (17.8)	1.05 ± 0.02 (1.07)	0.65 ± 0.10 (0.72)	
100	21.0 ± 0.9 (22.0)	15.6 ± 1.1 (17.4)	1.07 ± 0.03 (1.10)	0.71 ± 0.03 (0.73)	

Table 1: Performance Parameters. Performance metrics of devices made with and without formic acid. Average cell efficiencies are presented with the standard deviation. Values for the champion devices of each acid concentration are given in brackets.

To investigate if a similar effect can be obtained using both a different perovskite, as well as a fast crystallisation approach, we apply this methodology to the solvent quenching fabrication process. Here, we vary the formic acid concentration in the DMF used to fabricate a precursor solution of the mixed halide, mixed cation perovskite $FA_{0.83}MA_{0.17}Pb(I_{0.83}Br_{0.17})_3$, films of which are most frequently fabricated through the solvent quenching process. As an initial test to see if there is any measureable effect on the optoelectronic properties of the films produced through this route, we perform photoluminescence quantum efficiency (PLQE) measurements, which provide an indication of the extent of non-radiative recombination in the films. We present these results in **Figure S15.** We see from these measurements that the addition of formic acid to the solvent results in an increase in PLQE of films fabricated from precursor solutions with concentrations of up to 7.5 vol.% FAH, reaching a maximum PLQE of 20.5%. After this point the PLQE begins to decrease. With

this processing route, the crystallisation is rapid and largely controlled by the deposition of the anti-solvent, hence we do not expect to see as significant changes in morphology or crystallinity as we observed with the conventional one-step spin-coating. From SEM images (**Figure S16**) we see that in films both with and without formic acid, we have uniform coverage and very similar grain sizes. We show the XRD of these films in **Figure S17** and show that the crystallinity of the films (as determined by the width and intensity of the 110 peak) is very similar, although the exact orientation of the crystals (as inferred from the relative intensity of the different XRD peaks) appears to be slightly different. Having identified the optimal formic acid concentration from the PLQE measurements, we proceed to incorporate these films into full solar cells. Through the addition of 7.5 vol.% of acid to the precursor solution, we are able to obtain a maximum power conversion efficiency of 19.9%. We present the current-voltage curves and stabilised efficiencies in **Figure 7**. As with the $CH_3NH_3PbI_{3-x}Cl_x$ perovskite devices discussed earlier, while devices fabricated from both the neat and acidified precursor solutions exhibit hysteresis, we observe a reduction in the hysteresis with the addition of formic acid (forward and reverse scans are shown in **Figure S18**).

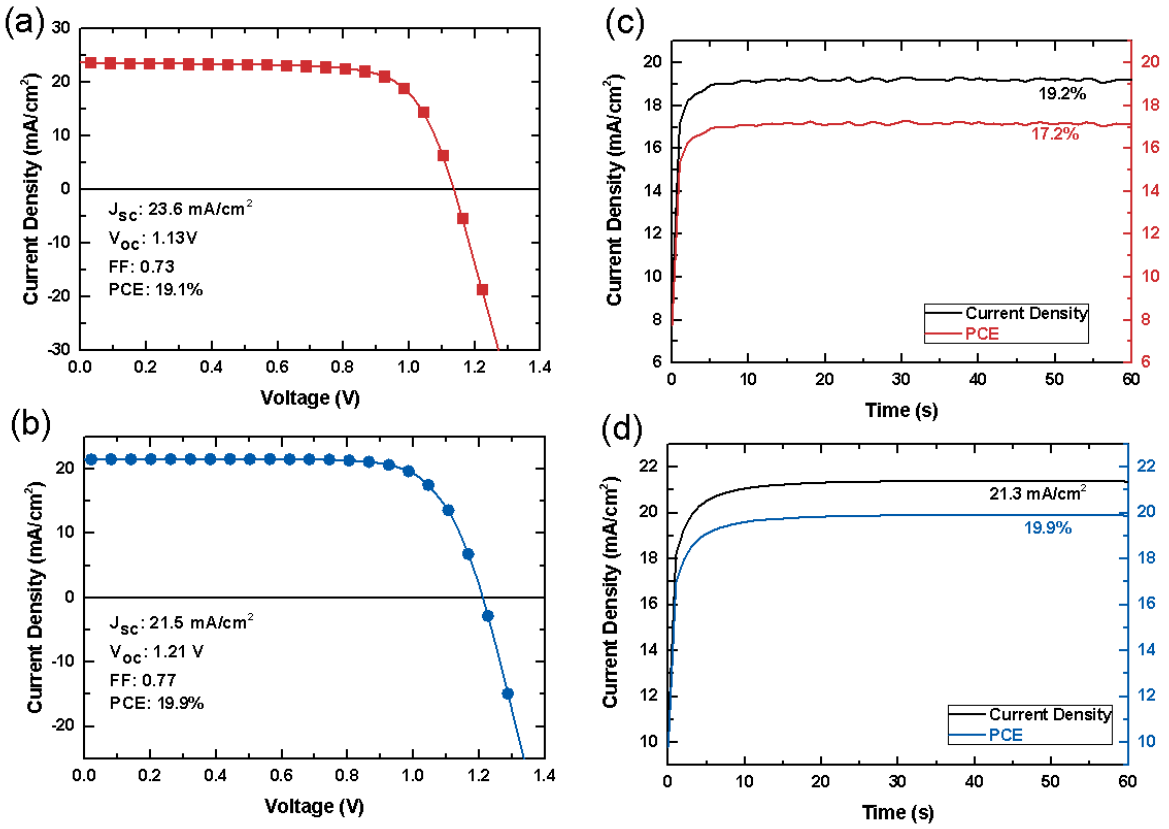

Figure 7: Current-Voltage Characteristics. Current-voltage curves of $FA_{0.83}MA_{0.17}Pb(I_{0.83}Br_{0.17})_3$ perovskite solar cells fabricated from a (a) neat precursor solution and an (b) acidified precursor solution. The corresponding stabilised currents and efficiencies are shown in (c) and (d).

Here, we see that much like in the case of the $CH_3NH_3PbI_{3-x}Cl_x$ perovskite, we see a noticeable increase in the open circuit voltage which can be obtained with the addition of formic acid. By adding formic acid to the precursor solution, and thus tuning the "age" of the DMF, we are able to achieve reduce the voltage loss in these perovskite devices by 70-80 mV. To confirm that these gains in open circuit voltage are indeed due to improvements in the quality of the perovskite layer and not to an incidental change in the underlying SnO_2 layer, we have performed experiments in which the SnO_2 layer is pre-treated with a DMF/FAH mixture and dried at 100 °C for 10 min before the deposition of the perovskite layers. We show the results of these experiments in **Figures S19 and S20**. At low formic acid concentrations we see very little to no effect on the voltage of the devices. However, at higher

concentrations we see a decrease in the voltage, suggesting that the increases which we observe in our devices are indeed due to improvements in the quality of the perovskite layers deposited. In the case of the $FA_{0.83}MA_{0.17}Pb(I_{0.83}Br_{0.17})_3$ which has a band gap of approximately 1.57 eV (See **Figure S21**), we obtain the lowest yet reported loss-in-potential from band gap to V_{OC} of only 360mV. To the best of our knowledge, the lowest reported loss-in-potential reported for perovskite solar cells to date is 390 mV.[35] We show the EQE for this device in **Figure S22**. This, in combination with the PLQE results, indicates that there is a significant reduction in the non-radiative recombination taking place within the perovskite film. We note however, that there is a significant reduction in the short circuit current density upon formic acid addition, this may in part be due to a significant reduction of film thickness even though the overall concentration of the precursor solution remains constant. While the exact cause of this phenomenon is under investigation, we postulate that this is in part due to a reduction in the concentration of colloids in the solution. Nevertheless, through these results, we show that the role of solvent pH in the crystallization of perovskite films is crucial not only to one-step, slow crystallization methods, but also the widely used solvent quenching method; and importantly, illuminates a path to achieving efficient, low voltage-loss perovskite photovoltaics.

Conclusions:

Using thymol blue as an indicator, we have shown through spectrophotometric measurements how the pH of DMF changes over time. We have also shown that the addition of commonly used acidic additives such as hydrohalic acids and HPA, act to increase the rate of hydrolysis of DMF, causing the production of dimethylamine and consequently, increase the basicity of

the solution. Through performing DLS measurements on neat and acidified DMF-based perovskite precursor solutions, we have shown that the addition of HCl, HI, HPA and formic acid all cause the dissolution of colloids in the perovskite precursor solution, and have also identified irreversible changes in DMF as a result of acid addition. We postulate that the production of dimethylamine, as a result of the thermal degradation and/or hydrolysis of DMF, plays an important role in the dissolution of colloids, which in turn results in enhanced film quality. By using formic acid as an additive to the perovskite precursor solution, we are able to artificially "age" the DMF solution without introducing excess halide or phosphorus into the films, thereby eliminating another potential variable in perovskite processing. Through the addition of an optimal concentration of formic acid to perovskite solutions made using anhydrous DMF, we are able to reproducibly obtain device efficiencies of over 18% for the $CH_3NH_3PbI_{3-x}Cl_x$ perovskite, and approach stabilised efficiencies of close to 20% with the mixed cation, mixed halide perovskite $FA_{0.83}MA_{0.17}Pb(I_{0.83}Br_{0.17})_3$. The effects of DMF degradation on the quality and reproducibility of perovskite-based devices have been largely unexplored. With this study, we have identified how the degradation of DMF through hydrolysis and thermal decomposition increases the solubility of the perovskite salts. This, in turn, causes a reduction in both the size and concentration of colloids in the precursor solution, resulting in the production of perovskite films with larger domains and more highly oriented crystals. By identifying the correlation between DMF degradation, solution pH, and perovskite crystallisation we show a facile method with which to not only increase the reproducibility of perovskite-based optoelectronic devices, but also to greatly reduce the voltage losses which occur in such devices.

Author Contributions:

N.N., B.W, and H.J.S. conceived the experiments. N.N., M.C, A.J.R, S.F., D.P.M, J.B.P and B.W. conducted the experiments. N.N. wrote the original draft of the manuscript. H.J.S supervised the project. M.B.J provided equipment and lent expertise. All authors have contributed to the final version of the manuscript.

Acknowledgements:

This work was funded by the Engineering and Physical Sciences Research council (EPSRC) programme grant EP/P02484X/1. B.W. acknowledges funding from the European Commission via a Marie Skłodowska-Curie individual fellowship (REA grant number: 706552-APPEL). The authors thank Dr.Avynash Bhagaloo, Dr. Reignier M. Jeffrey, Dr. Severin N. Habisreutinger and Dr. Pabitra K. Nayak for helpful discussions. The authors declare no competing financial interests.

References:

1. Z.-K. Tan, R. S. Moghaddam, M. L. Lai, P. Docampo, R. Higler, F. Deschler, M. Price, A. Sadhanala, L. M. Pazos, D. Credgington, F. Hanusch, T. Bein, H. J. Snaith and R. H. Friend, Nat Nano, 2014, 9, 687-692.

2. F. Deschler, M. Price, S. Pathak, L. E. Klintberg, D.-D. Jarausch, R. Higler, S. Hüttner, T. Leijtens, S. D. Stranks, H. J. Snaith, M. Atatüre, R. T. Phillips and R. H. Friend, The Journal of Physical Chemistry Letters, 2014, 5, 1421-1426.

3. N. R. E. L. (NREL), Best Research-Call Efficiencies, http://www.nrel.gov/ncpv/images/efficiency_chart.jpg).

4. H.-S. Kim, C.-R. Lee, J.-H. Im, K.-B. Lee, T. Moehl, A. Marchioro, S.-J. Moon, R. Humphry-Baker, J.-H. Yum, J. E. Moser, M. Gratzel and N.-G. Park, Sci. Rep., 2012, 2.

5. M. M. Lee, J. Teuscher, T. Miyasaka, T. N. Murakami and H. J. Snaith, Science, 2012, 338, 643-647.

6. J. M. Ball, M. M. Lee, A. Hey and H. Snaith, Energy & Environmental Science, 2013.

7. S. D. Stranks, G. E. Eperon, G. Grancini, C. Menelaou, M. J. P. Alcocer, T. Leijtens, L. M. Herz, A. Petrozza and H. J. Snaith, Science, 2013, 342, 341-344.

8. H. J. Snaith, The Journal of Physical Chemistry Letters, 2013, 4, 3623-3630.

9. J. Burschka, N. Pellet, S.-J. Moon, R. Humphry-Baker, P. Gao, M. K. Nazeeruddin and M. Gratzel, Nature, 2013, 499, 316-319.

10. K. Wojciechowski, T. Leijtens, S. Siprova, C. Schlueter, M. T. Hörantner, J. T.-W. Wang, C.-Z. Li, A. K. Y. Jen, T.-L. Lee and H. J. Snaith, The Journal of Physical Chemistry Letters, 2015, 6, 2399-2405.

11. M. Liu, M. B. Johnston and H. J. Snaith, Nature, 2013, advance online publication.

12. O. Malinkiewicz, A. Yella, Y. H. Lee, G. M. Espallargas, M. Graetzel, M. K. Nazeeruddin and H. J. Bolink, Nat Photon, 2014, 8, 128-132.

13. N. K. Noel, S. N. Habisreutinger, B. Wenger, M. T. Klug, M. T. Horantner, M. B. Johnston, R. J. Nicholas, D. T. Moore and H. J. Snaith, Energy & Environmental Science, 2017, 10, 145-152.

14. N. J. Jeon, J. H. Noh, Y. C. Kim, W. S. Yang, S. Ryu and S. I. Seok, Nature materials, 2014, 13, 897-903.

15. J. P. Correa Baena, L. Steier, W. Tress, M. Saliba, S. Neutzner, T. Matsui, F. Giordano, T. J. Jacobsson, A. R. Srimath Kandada, S. M. Zakeeruddin, A. Petrozza, A. Abate, M. K. Nazeeruddin, M. Gratzel and A. Hagfeldt, Energy & Environmental Science, 2015, 8, 2928-2934.

16. M. Saliba, T. Matsui, J.-Y. Seo, K. Domanski, J.-P. Correa-Baena, M. K. Nazeeruddin, S. M. Zakeeruddin, W. Tress, A. Abate, A. Hagfeldt and M. Gratzel, Energy & Environmental Science, 2016, 9, 1989-1997.

17. J. T.-W. Wang, Z. Wang, S. Pathak, W. Zhang, D. W. deQuilettes, F. Wisnivesky-Rocca-Rivarola, J. Huang, P. K. Nayak, J. B. Patel, H. A. Mohd Yusof, Y. Vaynzof, R. Zhu, I. Ramirez, J. Zhang, C. Ducati, C. Grovenor, M. B. Johnston, D. S. Ginger, R. J. Nicholas and H. J. Snaith, Energy & Environmental Science, 2016, 9, 2892-2901.

18. M. T. Klug, A. Osherov, A. A. Haghighirad, S. D. Stranks, P. R. Brown, S. Bai, J. T. W. Wang, X. Dang, V. Bulovic, H. J. Snaith and A. M. Belcher, Energy & Environmental Science, 2017, 10, 236-246.

19. G. E. Eperon, G. M. Paterno, R. J. Sutton, A. Zampetti, A. A. Haghighirad, F. Cacialli and H. J. Snaith, Journal of Materials Chemistry A, 2015, 3, 19688-19695.

20. W. Zhang, S. Pathak, N. Sakai, T. Stergiopoulos, P. K. Nayak, N. K. Noel, A. A. Haghighirad, V. M. Burlakov, D. W. deQuilettes, A. Sadhanala, W. Li, L. Wang, D. S. Ginger, R. H. Friend and H. J. Snaith, Nat Commun, 2015, 6.

21. J. H. Heo, D. H. Song, H. J. Han, S. Y. Kim, J. H. Kim, D. Kim, H. W. Shin, T. K. Ahn, C. Wolf, T.-W. Lee and S. H. Im, Advanced Materials, 2015, 27, 3424-3430.

22. F. Wang, H. Yu, H. Xu and N. Zhao, Advanced Functional Materials, 2015, 25, 1120-1126.

23. J.-Y. Seo, T. Matsui, J. Luo, J.-P. Correa-Baena, F. Giordano, M. Saliba, K. Schenk, A. Ummadisingu, K. Domanski, M. Hadadian, A. Hagfeldt, S. M. Zakeeruddin, U. Steiner, M. Grätzel and A. Abate, Advanced Energy Materials, 2016, 6, 1600767-n/a.

24. J. Xu, A. Buin, A. H. Ip, W. Li, O. Voznyy, R. Comin, M. Yuan, S. Jeon, Z. Ning, J. J. McDowell, P. Kanjanaboos, J.-P. Sun, X. Lan, L. N. Quan, D. H. Kim, I. G. Hill, P. Maksymovych and E. H. Sargent, Nature Communications, 2015, 6, 7081.

25. X. Gong, M. Li, X.-B. Shi, H. Ma, Z.-K. Wang and L.-S. Liao, Advanced Functional Materials, 2015, 25, 6671-6678.

26. G. E. Eperon, S. D. Stranks, C. Menelaou, M. B. Johnston, L. M. Herz and H. J. Snaith, Energy & Environmental Science, 2014, 7, 982-988.

27. D. P. W. McMeekin, Zhiping; Rahaman, Waqaas; Pulvirenti, Federico, Patel, Jay B.; Noel, Nakita K.; Marder, Seth R.; Johnston, Michael B.; Herz, Laura M.; Snaith, Henry J., Advanced Materials, 2017, DOI: 10.1002/(ISSN)1521-4095.

28. J. H. Heo, H. J. Han, D. Kim, T. K. Ahn and S. H. Im, Energy & Environmental Science, 2015, 8, 1602-1608.

29. C. M. M. Soe, C. C. Stoumpos, B. Harutyunyan, E. F. Manley, L. X. Chen, M. J. Bedzyk, T. J. Marks and M. G. Kanatzidis, ChemSusChem, 2016, 9, 2656-2665.

30. S. Liu, C. Wang, H. Zhai and D. Li, Journal of Molecular Structure, 2003, 654, 215-221.

31. T. Cottineau, M. Richard-Plouet, J.-Y. Mevellec and L. Brohan, The Journal of Physical Chemistry C, 2011, 115, 12269-12274.

32. R. S. Brown, A. J. Bennet and H. Slebocka-Tilk, Accounts of Chemical Research, 1992, 25, 481-488.

33. G. Long and M. Meek, Concise international chemical assessment document (ISSN 1020-6167, 2001, 31.

34. P. K. Nayak, D. T. Moore, B. Wenger, S. Nayak, A. A. Haghighirad, A. Fineberg, N. K. Noel, O. G. Reid, G. Rumbles, P. Kukura, K. A. Vincent and H. J. Snaith, Nature Communications, 2016, 7, 13303.

35. M. Saliba, T. Matsui, K. Domanski, J.-Y. Seo, A. Ummadisingu, S. M. Zakeeruddin, J.-P. Correa-Baena, W. R. Tress, A. Abate, A. Hagfeldt and M. Grätzel, Science, 2016, DOI: 10.1126/science.aah5557.

36. H. Zhang and R. H. Byrne, Marine Chemistry, 1996, 52, 17-25.

37. R. A. Cox, Angewandte Chemie International Edition, 2013, 52, 7638-7638.

38. J. A. Marsella, in Kirk-Othmer Encyclopedia of Chemical Technology, John Wiley & Sons, Inc., 2000, DOI: 10.1002/0471238961.0409130513011819.a01.

39. K. Yan, M. Long, T. Zhang, Z. Wei, H. Chen, S. Yang and J. Xu, Journal of the American Chemical Society, 2015, 137, 4460-4468.

40. Z. Zhou, Z. Wang, Y. Zhou, S. Pang, D. Wang, H. Xu, Z. Liu, N. P. Padture and G. Cui, Angewandte Chemie International Edition, 2015, 54, 9705-9709.

41. E. H. Anaraki, A. Kermanpur, L. Steier, K. Domanski, T. Matsui, W. Tress, M. Saliba, A. Abate, M. Gratzel, A. Hagfeldt and J.-P. Correa-Baena, Energy & Environmental Science, 2016, 9, 3128-3134.

42. H. Tsai, W. Nie, Y.-H. Lin, J. C. Blancon, S. Tretiak, J. Even, G. Gupta, P. M. Ajayan and A. D. Mohite, Advanced Energy Materials, 2017, DOI: 10.1002/aenm.201602159, 1602159-n/a.

43. W. Nie, H. Tsai, R. Asadpour, J.-C. Blancon, A. J. Neukirch, G. Gupta, J. J. Crochet, M. Chhowalla, S. Tretiak, M. A. Alam, H.-L. Wang and A. D. Mohite, Science, 2015, 347, 522-525.

44. H. Tsai, W. Nie, J.-C. Blancon, C. C. Stoumpos, R. Asadpour, B. Harutyunyan, A. J. Neukirch, R. Verduzco, J. J. Crochet, S. Tretiak, L. Pedesseau, J. Even, M. A. Alam, G. Gupta, J. Lou, P. M. Ajayan, M. J. Bedzyk, M. G. Kanatzidis and A. D. Mohite, Nature, 2016, 536, 312-316.

TOC GRAPHIC:

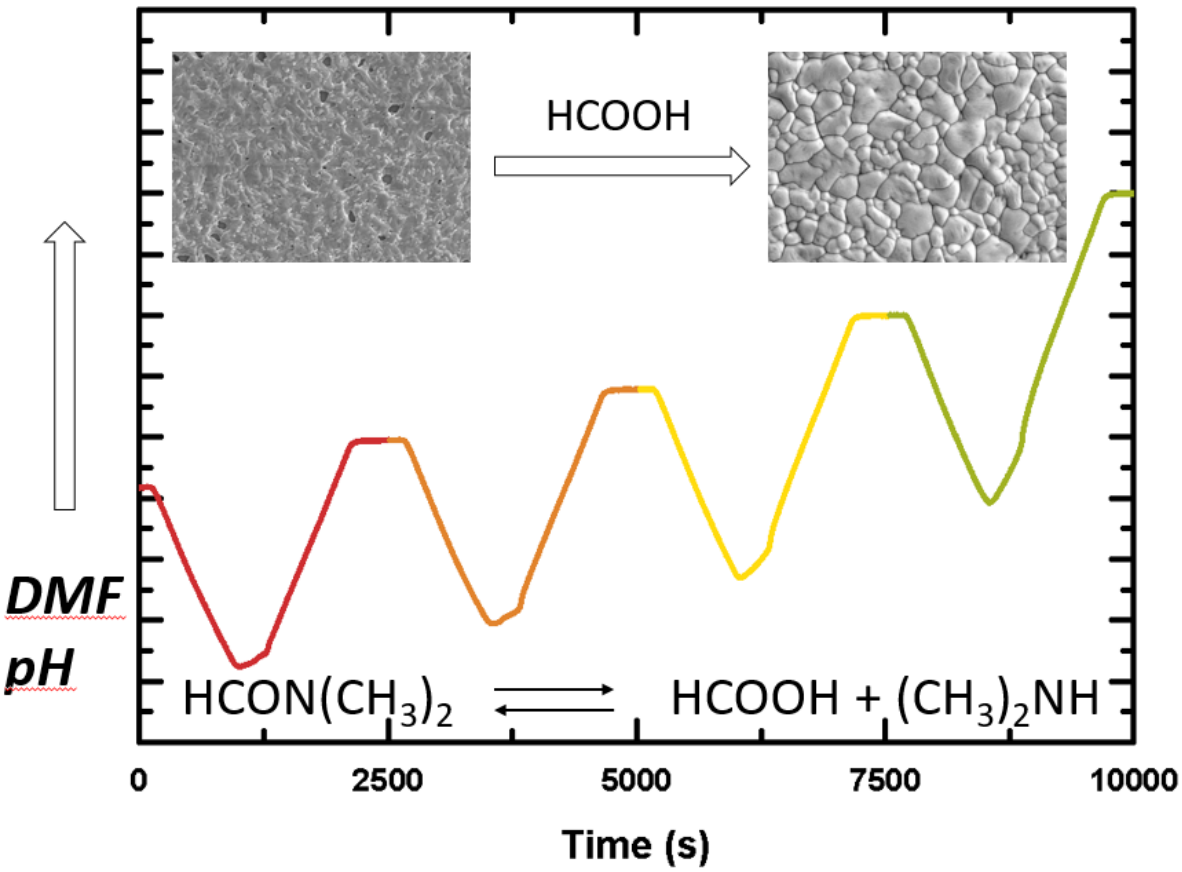
HCOOH
DMF
pH
HCON(CH3)2
HCOOH + (CH3)2NH
0
2500
5000
7500
10000
Time (s)